Zilstra, A., & Johnson, D. A. (2024). Computational Aeroacoustic Prediction of Tonal Noise for Low Reynolds Number Airfoils. In 30th AIAA/CEAS Aeroacoustics Conference. American Institute of Aeronautics and Astronautics. https://doi.org/10.2514/6.2024-3362

Computational Aeroacoustic Prediction of Tonal Noise for Low Reynolds Number Airfoils

Alison Zilstra * and David A. Johnson†
University of Waterloo, Waterloo, Ontario, N2L 3G1, Canada

Airfoils operating in low Reynolds number, Re, conditions can generate tonal aeroacoustic noise due to the laminar or transitional boundary layer (BL) at the airfoil trailing edge (TE). At modest Re of less than 1×10^5, an elongated laminar separation bubble (LSB) can occur near the TE which adds complexity to the BL transition and also generates tonal noise. Computational fluid dynamic and computational aeroacoustic simulations of the SD 7037 airfoil at $Re = 4.1\times10^4$ are completed to study this phenomenon. The numerical methods used are incompressible wall-resolved large eddy simulation (LES) and the Ffowcs-Williams and Hawkings acoustic analogy, with the results of both methods validated against experimental data. The LES simulation of the airfoil BL development is critical to the tonal noise prediction and the accuracy of the predicted tones were assessed for a series of mesh refinements in the near-wall and separated BL regions. The mesh refinements in the regions of BL separation resulted in the correct simulation of the LSB and the associated aeroacoustic tonal noise for 1° angle of attack (AOA). Simulations at higher AOAs showed the sensitivity of the transient BL behaviour to the mesh refinements in the BL, while the time-averaged BL behaviour remained stable. Spectral analysis of the velocity in the BL determined that the source of the tone originates from the Tollmien-Schlichting wave frequency in the attached laminar BL, which is then amplified by the Kelvin-Helmholtz instability that forms in the LSB. The accurate tonal noise prediction occurred in the absence of the acoustic feedback mechanism.

I. Introduction

Aeroacoustic sound waves are generated in response to the fluctuating forces in a turbulent flow or from fluid flow around an object. Any undesired sound generated in this process is referred to as aeroacoustic noise and aeroacoustic design aims to reduce the source strength or to create new technologies to dampen the noise or interfere with its propagation. A heavily researched area of aeroacoustics is airfoil self-noise, which is useful for any application of wings or blades, such as compressor and turbine cascades, helicopter rotors, HVAC fans, wind turbines and small-scale propellers for drones. One application of interest is the flow around low Reynolds number (Re) airfoils, defined as a chord based Re of less than 5×10^5, which often generate tonal noise due to the flow structures present as the boundary layer (BL) transitions to turbulence.

A. Airfoil Self-Noise

Airfoil self-noise is caused by the transient flow behaviours in the BL that form along the airfoil surface, with the majority of the noise radiating from the sharp trailing edge (TE) [1]. The frequency content and amplitude of the generated noise is dependent on the development of the BL when it reaches the TE. A turbulent BL will produce broadband noise, described as a swishing sound, due to turbulent eddies passing the trailing edge of the airfoil [2]. A laminar BL creates broadband noise with additional tonal components, which are elevated noise for a narrow frequency range that can be described as a whistling noise. The noise is produced due to the high spanwise coherence of the structures in the laminar BL as it passes over the TE and the regular frequency vortex shedding occurring in the near wake. Additionally, there is often discussion of an acoustic feedback mechanism [1] or acoustic coupling [2, 3] for the laminar BL TE noise mechanism where acoustic waves travel upstream to the unstable laminar BL and initiate the formation of BL structures at the tonal noise frequency. The tonal TE noise is best mitigated by tripping the BL to cause turbulent flow, however, this mitigation method is not ideal for airfoils designed for use in low Re applications, since the airfoil is optimized to take advantage of the laminar BL.

*PhD Candidate, Wind Energy Group, Mechanical and Mechatronics Engineering, 200 University Ave W
†Professor, Wind Energy Group, Mechanical and Mechatronics Engineering, 200 University Ave W

B. Low Reynolds Number Airfoils

Modern airfoils specifically designed for operation at a low Re are most commonly cambered airfoils and are used in applications such as small wind turbines (SWT), micro air vehicles (MAV) and unmanned air vehicles (UAV). These low Re airfoils are designed to operate in conditions where a significant portion of the airfoil BL is laminar or transitional and often transitional separated flow, shown in Fig. 1, is unavoidable which can impact both the aerodynamic and aeroacoustic performance. Transitional separated flow, also known as a laminar separation bubble (LSB), occurs when the adverse pressure gradient causes BL separation due to the low momentum of the laminar BL [4, 5]. The high velocity gradient between the separated BL and the reverse flow near the wall triggers a Kelvin-Helmholtz (K-H) instability that generates spanwise vortices, known as K-H rolls [6].

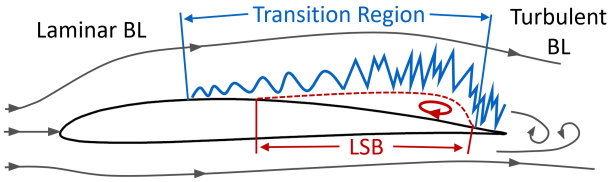

Fig. 1 Boundary layer transition (blue) over a cambered airfoil, including LSB details (red) [7]

The frequency of the K-H instability has been found to be similar in magnitude to the frequency of the Tollmien-Schlichting (T-S) waves that develop during the start of the BL transition in the attached BL [8, 9]. As is shown in Fig. 1, the LSB often forms after the attached laminar BL has begun to transition and structures that develop within the attached BL have influence on the growth of the K-H rolls and the frequency at which they form. A correlation developed using stability theory on a flat plate can be used to approximate the T-S wave frequency using the displacement thickness and edge velocity of the BL [10], though this has limited applicability for airfoils where the BL develops under the presence of large pressure gradients. The frequency of the K-H rolls can be made dimensionless using a Strouhal number based on the BL properties at the location of separation, which results in a range of 0.005 to 0.016 [9]. The Strouhal number is defined as

$$St_{\theta s} = \frac{f\theta_s}{U_{es}} \tag{1}$$

where f is the K-H roll frequency, θ_s is the momentum thickness of the BL at the location of separation and U_{es} is the edge velocity of the BL at separation.

The growth of the K-H instability and formation of the K-H rolls generates turbulence that increases the near-wall momentum exchange, causing BL reattachment as a turbulent BL [9, 11]. In some cases the laminar separation occurs close to the airfoil TE, such that the BL is unable to reattach and therefore has a separated BL at the TE [7, 12]. This is problematic from an aeroacoustic noise perspective, since the transitional separated BL has regularly forming structures with associated strong pressure fluctuations that will generate tonal noise as they pass the TE [13].

C. Computational Aeroacoustics

The design of noise mitigation strategies for this type of low Re airfoil self-noise requires a detailed understanding of the type of flow structures occurring in the LSB and their associated frequencies. Numerical methods can be used to fill the gaps in knowledge that currently exist from experimentation, so long as the simulations are well validated. Computational aeroacoustic (CAA) simulations require a detailed simulation of the transient flow behaviour around the airfoil which is obtained using computational fluid dynamics (CFD). In direct CAA, also called direct noise computation (DNC), the aerodynamic and aeroacoustic fields are calculated simultaneously using a compressible CFD method which is capable of capturing the effect of the sound waves on the flow field. This method is challenging and computationally expensive to complete since it requires high-fidelity compressible simulations to prevent excess dissipation of the low energy acoustic field [14].

An acoustic analogy simplifies the CAA solution by assuming that a bounded region in the flow can be solved as an acoustic source and then linearly propagated in the surrounding area using the general wave equation [15]. It has been well established by those in the CAA field that for low Mach number flows and flows where the propagation distance is large, the acoustic analogy is a preferred option compared to more computationally expensive models, especially when considering rotating flows such as helicopters and wind turbines [16, 17]. Acoustic analogies, such

as the Ffowcs-Williams and Hawkings (FW-H) acoustic analogy [18, 19], are highly dependent on the quality of the input data from the CFD simulation, which predicts the small scale transient fluctuations in the airfoil BL. For low Re airfoils, the simulation of the transitional BL must be thoroughly validated to ensure the small scale velocity and pressure fluctuations are captured by the CFD simulation.

Detailed transient CFD simulations of transitional separated flow over low Re airfoils either employ direct numerical simulation (DNS) [11, 20–22] or large eddy simulation (LES) [6, 20, 23–26] to capture the small scale transient behaviour in the BL and LSB. LES is an accessible alternative to the computationally expensive DNS method, and therefore is preferable for aeroacoustic design purposes. As with most applications of LES, the mesh sizing and simulation parameters required to generate high quality transient data are highly dependent on the geometry and flow conditions. This is especially true for airfoils operating at a modest Re of less than 1×10^5, which are more likely to have an elongated LSB [7, 12] and experience the tonal noise associated with the interaction of structures in the transitional separated BL with the TE. Prior investigations by the authors had agreement of the time-averaged aerodynamic results including lift coefficient, C_L, and pressure coefficient, C_p, however the accuracy of the tonal noise prediction was either inconsistent across different angles of attack (AOA) [13] or the tone frequency was overly sensitive to simulation parameters [27]. It was determined that the time-averaged aerodynamic results can be accurate while there are errors present in the small-scale transient behaviour responsible for tonal noise, even when considering the complex transient behaviour of a LSB. This poses a challenge for the use of this method for designing noise mitigation strategies, since traditional techniques for validating CFD simulations fall short when that data is to be used for CAA prediction.

This work focuses on the simulation of the SD 7037 cambered low Re airfoil which is known to experience transitional separated flow that generates tonal noise at two dominant frequencies. The simulations are performed using LES for the transient flow field calculation and FW-H for the aeroacoustic noise prediction, with both the flow field and aeroacoustic results validated against experimental data [12, 28]. The dependence of the FW-H aeroacoustic prediction on the transient LES flow field simulation places high importance on the quality of the LES simulation. The detailed time-averaged validation of the LES has been published previously [7] with a particular focus on the size and location of the LSB. This work studies the impact of further BL mesh refinements on the transient prediction of the airfoil BL and the resulting prediction of the tonal aeroacoustic noise.

II. Methodology

The simulations were performed using ANSYS Fluent, release 21.2, with LES as the CFD model and FW-H as the acoustic analogy. The FW-H analogy requires the selection of a surface as the source of the transient pressure fluctuations that generate the sound, and a receiver location to propagate the sound towards. For these simulations, the surface of the airfoil is selected as the source, and the experimental microphone location [28] is chosen as the receiver. The FW-H model requires the input of accurate transient flow data on the surface of the airfoil, therefore wall-resolved LES is used with the dynamic Smagorinsky-Lilly subgrid scale (SGS) model. The mass and momentum conservation equations were solved in the incompressible form, as compressibility is not required in this low Re case to resolve the BL behaviour [7]. The flow was initialized with a RANS model ($\gamma - Re_{\theta t}\ k - \omega$) to improve LES convergence time and the simulations were run using 128 cores on a high performance compute cluster in the Digital Research Alliance of Canada network [29].

The selected airfoil profile is the SD 7037 airfoil [30] which is designed for low Re applications and is well suited for the use on a SWT. The simulations were performed at a Re of 4.1×10^4 with a chord length of $c = 25.8mm$, for which there is experimental data available for the validation of the aerodynamic [12] and aeroacoustic [28] behaviours. The experimental data measured at a location $3.0c$ below the quarter-chord of the airfoil show that tonal noise is produced at AOAs lower than 5°, with the loudest tone of 120 dB occurring at 1° AOA [28]. There are also two tone frequencies that appear across all AOAs in the experimental data, where the dominant tone frequency at 1° and 5° AOA is 3.4 kHz and at 0°, 2° and 3° the tone is at 4.1 kHz. The simulations were completed at 1°, 3° and 5° AOA to cover the full range of aerodynamic and aeroacoustic behaviour for the airfoil during tonal noise generation. The simulation geometry and aerodynamic parameters are summarized in Table 1 with the detailed numerical method described in the following sections.

The simulations are completed using three versions of the mesh which progressively refine the BL region to reduce the filter length and improve the transient BL prediction. The simulations are run for a minimum of $0.01s$ at a time step, Δt, of $2 \times 10^{-6}s$ or $4 \times 10^{-6}s$ to collect at least 92 chord-based mean flow residence times (MFRT) of data. The acoustic prediction and the time-averaged parameters are processed omitting the initialization of the domain, which is 18 to 24 MFRT depending on the domain size. The transient analysis of the BL transition in the LSB region is completed for 18

Table 1 Geometric and aerodynamic details

Airfoil Profile		SD 7037	Angle of Attack	α	1°, 3°, 5°
Chord	c	0.0258 m	Inflow Velocity	U_∞	23.84 m/s
Span	b	$0.2c$	Reynolds Number	Re	4.1×10^4
Radius	R	$8c$ to $12c$	Mach Number	Ma	0.07
Downwind Length	L	$10c$ to $12c$	Turbulent Intensity	I	1%

to 37 MFRT, where signals of the velocity components and static pressure are collected at chordwise spacings of $0.05c$ and at a wall-normal distance from the airfoil surface of $3 \times 10^{-2}c$ and $4 \times 10^{-3}c$. The global x,y,z-coordinates are converted to s,n,z-coordinates where the s-velocity is tangent to the local airfoil curvature and the n-velocity is normal to the curvature. A spectral analysis of the n-velocity is used to determine the change in transient BL behaviour with the different mesh versions and determine the relationship between flow frequencies and the tonal TE noise frequencies.

A. Domain Geometry

The fluid domain surrounding the airfoil is a C-mesh as shown in Fig. 2a which is an ideal geometry for a structured mesh since the curved surface aligns well with the curved surface of the airfoil. The dimensions of the domain are scaled with the chord length, c, where the radius, R, and downstream length, L, ranged between $8c$ and $12c$ to optimize computational resources as mesh refinements were completed. The reduction of boundary offset from $R = L = 12c$ to $R = 8c$ and $L = 10c$ resulted in no observed change to the flow around the blade. A C-mesh of $R = 4c$ and $L = 10c$ has previously been used by Smith and Ventikos [20] for DNS and LES simulations of a LSB on a NACA 0012 airfoil at a Re of 1×10^5.

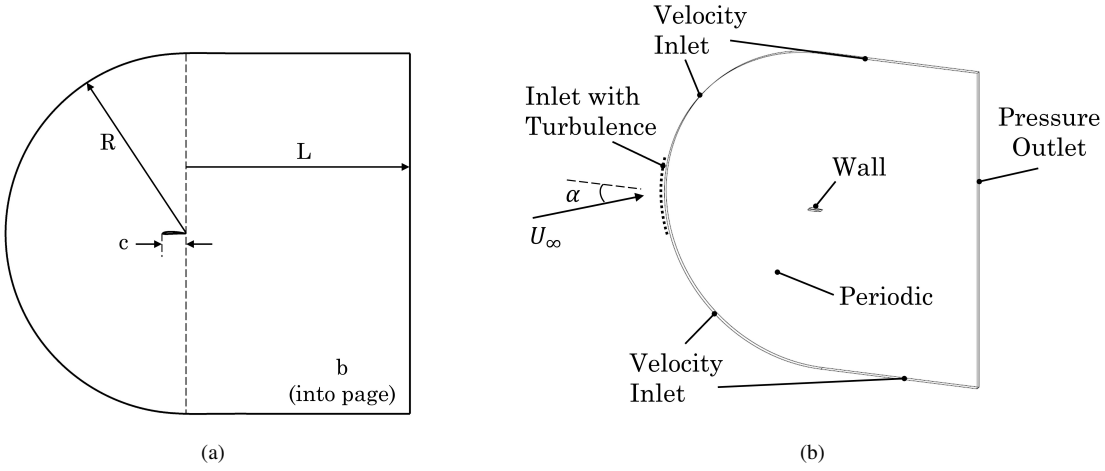

Fig. 2 Diagrams of (a) computational domain geometry and (b) simulation boundary conditions

The spanwise length of the domain, b, was set at a length of $0.2c$ after tests with $b = 0.4c$ showed no impact on simulation of the BL transition. The spanwise extent is consistent with the $0.2c$ commonly seen in simulations of transitional flow over symmetric NACA airfoils [20, 21] and cambered airfoils [25, 26, 31]. The summary of the geometry details for the computational domain can be found in Table 1 along with the aerodynamic parameters for the simulation case.

B. Boundary Conditions

The boundary conditions used for the simulation domain are shown in Fig. 2b. The airfoil surface is defined as a no-slip wall and the vertical outlet is defined as a pressure outlet. The curved and horizontal edges of the domain are set as velocity inlets, where the free-stream velocity of $U_\infty = 23.54$ m/s is at an angle with the horizontal corresponding to the airfoil AOA, α. The application of inflow turbulence at the inlet is explained in the following section.

The spanwise boundary condition has the potential to influence the formation of the spanwise structures in the transitioning BL and is set as a periodic boundary condition for these simulations. The periodic boundary condition is commonly used for simulations of low Re transitional separated flow with a spanwise extent of $0.2c$ [20, 21, 25, 26, 31]. The spanwise extent and spanwise boundary condition are of greater concern for compressible DNC simulations, which requires the development and propagation of spanwise acoustic waves. The current simulations generate the aeroacoustic prediction through incompressible LES with an acoustic analogy and therefore the current selection of the periodic boundary condition will not introduce any problematic spanwise aeroacoustic patterns.

1. Inflow Turbulence

A known issue with LES is the difficulty of generating an accurate replication of inflow turbulence conditions, since the model can be quite dissipative [24, 32]. Accurate turbulence generation is necessary for transitional separated flow since increasing turbulence has been shown to cause a decrease in the LSB length [11, 24, 26, 31]. Synthetic turbulence generation methods are generally favoured for practical applications [33], and are included in commercial computational fluid dynamics software packages. Roberts and Yaras [34] used a synthetic method built-in to ANSYS CFX to generate turbulence for the simulation of transitional separated flow on a flat plate. For this work, the ANSYS Fluent built-in Spectral Synthesizer method was chosen and the inflow turbulence was introduced in a $4.75c$ segment for $R = 12c$ and $3.16c$ segment for $R = 8c$ of the curved inlet located directly upstream of the airfoil, as shown in Fig. 2b. The mesh in this region was controlled to ensure the SGS filter length was smaller than the inflow turbulence length scale of 11 mm to prevent excessive dissipation. This method generated the desired level of inflow turbulence at the airfoil, while keeping the computational cost low by reducing the complexity of the calculations in the farfield of the domain. The turbulent intensity at the inlet is artificially increased to account for the dissipation that occurs between the inlet and the airfoil [24], which results in a turbulent intensity of 1% at a location 24 mm upstream of the LE as measured experimentally [12, 35]. Tests of the inlet turbulence dissipation determined the ideal specified inlet turbulent intensity to be 4.4% for domains with $R = 12c$ and 3.3% for domains with $R = 8c$.

C. Mesh and LES Filter Length

The structured hexahedral mesh is generated using the ICEM CFD package in ANSYS, which is ideal for strict control of the mesh sizing and expansion. The mesh sizing is important for LES not only to have sufficient resolution of the velocity and pressure gradients, but also because the subgrid filter length used is dependent on the mesh sizing where the subgrid filter length, Δ, is equal to the cubed root of the cell volume [36]. If the mesh sizing is coarse for the local length scales of the turbulence then the simulation will excessively dissipate the turbulence. The mesh versions 1 through 3 seek to improve the filter length in the low Re airfoil BL and details of each mesh version are summarized in Table 2.

Table 2 Mesh parameters for mesh versions 1-3

Mesh #	1	2	3
Radius, R	$12c$	$12c$	$8c$
Downwind Length, L	$12c$	$12c$	$10c$
Number of Elements	2.6×10^6	4.5×10^6	8.8×10^6
Chordwise Divisions	300	300	670
Spanwise Divisions	50	50	75
Inlet Turbulence, Tu	4.4%	4.4%	3.3%
Angle of Attack, α	1°, 5°	1°, 3°, 5°	3°, 5°
Time Step, Δt	4×10^{-6}	2×10^{-6}	4×10^{-6}

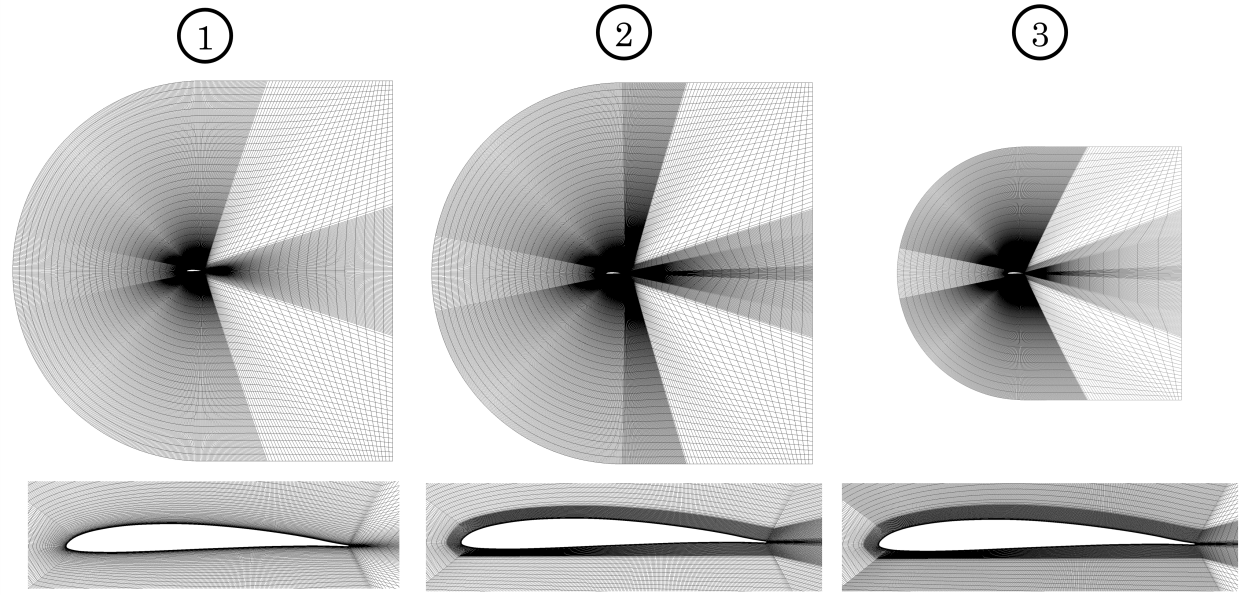

Fig. 3 Full domain mesh and close-up of airfoil for mesh versions 1-3

1. Mesh 1

The first mesh version, Mesh 1, consists of 2.6 million elements with 300 chordwise and 50 spanwise divisions with the mesh distribution shown in Fig. 3 and the geometric and simulation details summarized in Table 2. The first layer height at the airfoil surface is 0.005 mm with a wall-normal expansion ratio of 1.1, which results in a wall y^+ of less than 0.5 at the airfoil surface for all simulated AOAs, with an average y^+ of 0.21 for 1° AOA. Pope [37] suggests that accurate wall-resolved LES requires 80% of the turbulent kinetic energy to be resolved (i.e. not calculated through SGS modelling) which is based on the production range, or energy containing range, of the turbulent cascade where 80% of the energy is contained in eddies of that length scale. To achieve this in the BL, Pope recommends that the subgrid filter length Δ is on the order of the viscous length scale, δ_v, for $y^+ < 20$. Viscous lengthscale is defined as

$$\delta_v \equiv \nu \sqrt{\frac{\rho}{\tau_w}} \tag{2}$$

and is therefore dependent on the local shear stress, τ_w, and the fluid properties, ν and ρ, in the BL for each AOA simulated. Since $y^+ = y/\delta_v$, this is the basis of the criteria that the wall y^+ should be less than or equal to 1, however the true criteria is based on the volume which also depends on Δx^+ and Δz^+. Meeting this criteria requires an iterative mesh refinement process since the τ_w changes as the mesh is improved, though the region of highest important for this criteria is near the LE where the velocity in the BL is high, and therefore so is τ_w. After examining prior results for the 1° AOA case for Mesh 1 [7], the BL was found to meet this condition with $\Delta \leq 10\delta_v$ for the suction side BL and with an average of $2.4\delta_v$ at the surface and $4.5\delta_v$ at $y^+ = 20$.

2. Mesh 2

Mesh 2 consists of 4.5 million elements as shown in Fig. 3 and uses the same chordwise, spanwise and wall mesh distribution as Mesh 1. This mesh focuses on improving the resolution of the separated BL that occurs during the LSB where the BL is offset from the wall and therefore occurs in a coarser region of the mesh. To resolve this, the mesh distribution for Mesh 2 includes an additional band of uniform sized cells offset from the airfoil surface, achieved by halting the wall-normal mesh expansion in the regions of K-H roll formation. This region was measured from the results of Mesh 1 simulations at 1°, 5° and 7° AOAs [7] to be at wall-normal distance from $0.007c$ to $0.04c$ and can be seen as the darker band of cells surrounding the Mesh 2 airfoil in Fig. 3. A close up view of the BL mesh distribution is shown in Fig. 4a where the improved resolution has 40 nodes within the K-H roll region in comparison to the 15 in the same region for Mesh 1. Additionally, the near-wake region of the mesh was refined to allow for proper development of the vortex shedding at the airfoil TE as it relates to the tonal noise generation.

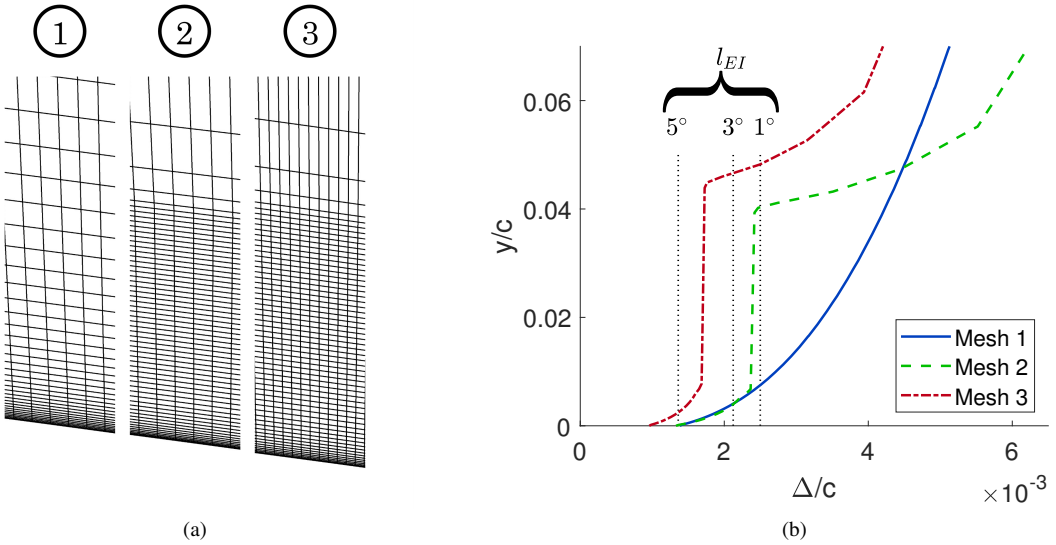

(a) (b)

Fig. 4 Improvements for mesh versions 1-3 of (a) wall-normal expansion at same location, and (b) filter length near the wall with approximate l_{EI} for the separated BL

3. Mesh 3

In order to improve the filter length in the separated region of the BL, the filter length criterion for free shear flows is applied to the regions where BL separation occurs. In these types of flows, Pope [37] recommends that the subgrid filter length, Δ, is "somewhat smaller" than l_{EI} which is defined as the length scale dividing the energy containing range and the inertial subrange of the turbulent cascade. The turbulent cascade definitions were generated for idealized isotropic turbulence, therefore they do not strictly apply to the developing turbulence that occurs during the K-H roll formation over the LSB. However, there are no other criteria to apply to the filter length for free shear flows, so it is assumed that the criteria will serve as a guideline for the LSB mesh. The energy containing range is defined as being between the integral length scale, l_0, and l_{EI}. The largest length scales in the flow, $\mathcal{L}$, can be approximated as $6l_0$ and also $l_{EI} \approx l_0/6$. Assuming that the K-H roll length scale, l_{K-H} (the spacing of the rolls) is close to $\mathcal{L}$, then $l_{EI} \approx l_{K-H}/36$. Therefore the new filter length criterion for the LSB region of the mesh is $\Delta < l_{K-H}/36$.

Using Mesh 2 results for 1°, 3° and 5° AOAs, the distance between the centres of the K-H rolls were measured for several different time steps. The spacing of the K-H rolls is smaller earlier in the LSB then increases as the roll grows in strength and at 5° AOA the minimum measured l_{K-H} was 1.26 mm with an average of 1.64 mm. Measurements estimated from mode 1 of the proper orthogonal decomposition (POD) of experimental data by Ghorbanishohrat [12] resulted in a values from 1.07 to 1.46 mm. Since the values from Ghorbanishohrat were lower than the values measured from the simulation of same AOA, the new mesh criteria uses the minimum measured l_{K-H} for each simulated AOA. At 1° AOA the minimum l_{K-H} was measured at 2.32 mm and was 1.97 mm for 3° AOA. The corresponding l_{EI} for each minimum l_{K-H} is shown in Fig. 4b as vertical dotted lines to compare the filter length in the K-H roll region with the new criterion. The previously refined K-H roll region from Mesh 2 meets this criterion for 1° AOA only since the filter length does not exceed the l_{EI} until after the top of the K-H roll region.

Mesh 3 was designed to meet this free shear flow criteria at AOAs higher than 1° to improve the LSB simulation and aeroacoustic prediction. This posed a challenge since Mesh 2 exceeded the desired filter length for 3° AOA before reaching the K-H roll region of the mesh, and the 5° AOA criterion was only met at the airfoil surface. Since the cells in this near wall region have the largest dimensions in the chordwise and spanwise direction, new nodes were added in those directions rather than further altering the resolution in the wall-normal direction. The chordwise nodes were increased from 300 to 670 (as shown in Fig. 4a) and the spanwise nodes were increased from 50 to 75. This results in Mesh 3 meeting the filter length requirement in the separated BL for 3° AOA, and also meets the requirement at 5° AOA when calculating l_{EI} using the average l_{K-H} rather than the minimum value. The total number of elements increased significantly, which required reduction of the boundary offsets of the C-mesh to $R = 8c$ and $L = 10c$ to not exceed memory requirements of the computer used to locally set up and post-process the simulations. The final number of elements in Mesh 3 is 8.8 million, with the other parameters summarized in Table 2.

III. Results

A. Aerodynamic Validation

The time-averaged validation of the LSB simulation is summarized through a comparison of the suction side pressure coefficient, C_p, with experimental PIV data [12] in Fig. 5. A fully-formed LSB can be located in a C_p plot from the indicative transition ramp [38], where the C_p levels off at the location of laminar separation, labelled S, then pressure recovery occurs to complete the ramp shape at reattachment, labelled R. The simulated locations of laminar BL separation and reattachment are determined using the time-averaged chordwise skin friction coefficient, C_f, where a negative C_f occurs due to the time-averaged reverse flow within the LSB. The 1° and 3° AOA simulations are both complex low Re cases where there is laminar BL separation with a transitional BL at the TE, rather than a fully-formed LSB with a reattached BL. The Mesh 2 simulation at 1° AOA shows no change in the time-averaged C_p in comparison to the Mesh 1 prediction and a minimal $0.01c$ downstream shift in the BL separation location (Fig. 5a). For the 3° AOA results in Fig. 5b, there is no change between the Mesh 2 and Mesh 3 results. The mesh improvements for the 1° and 3° AOA cases were intended to meet the filter length requirement of l_{EI} for the K-H rolls in the separated BL (see Fig. 4b), indicating that the mesh refinements in the region of K-H roll formation has not altered the time-averaged BL simulation.

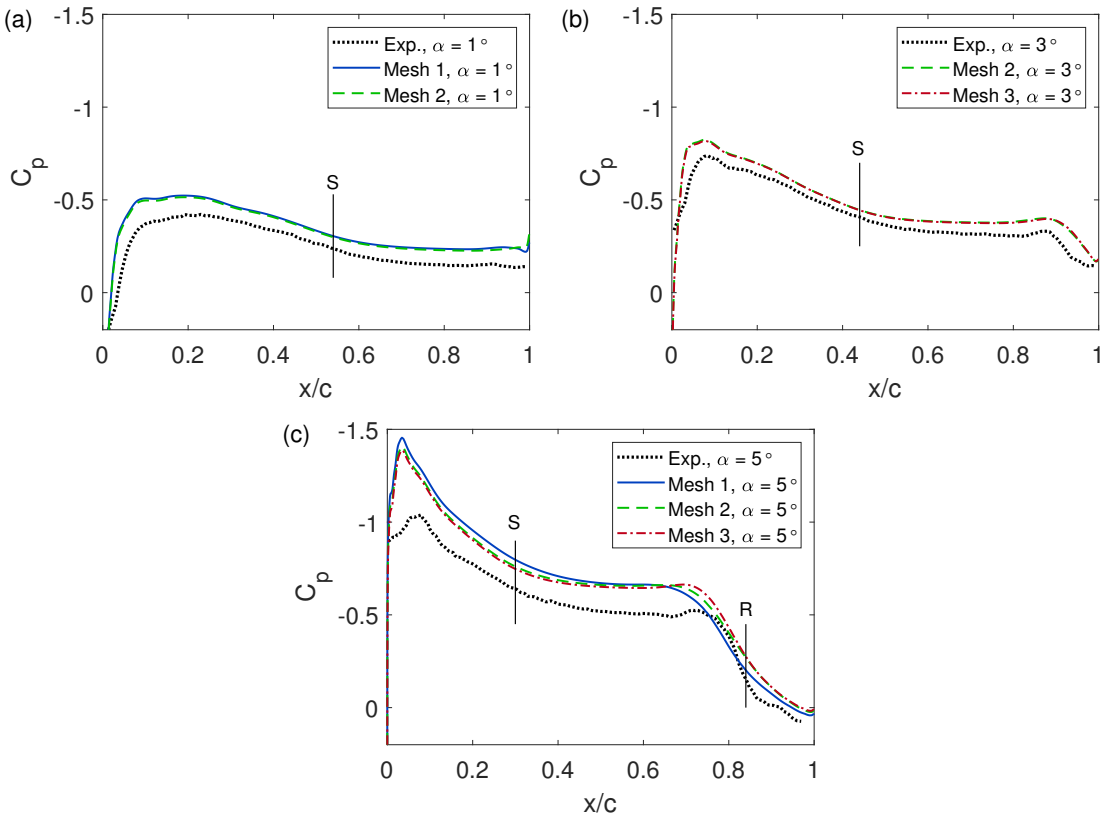

Fig. 5 Suction side pressure coefficient for (a) 1° AOA, (b) 3° AOA and (c) 5° AOA compared with experimental measurements [12] for Mesh 1 to 3. Locations of BL separation and reattachment are marked with S and R, respectively

There is variation in the time-averaged C_p across all three mesh versions at 5° AOA, as is shown in Fig. 5c. The refinements in Mesh 2 and Mesh 3 were intended to improve the K-H roll simulation in the region of BL separation, however they resulted in a lower C_p in the attached laminar BL and a $0.02c$ upstream shift in the location of laminar separation. More notably, the location where C_p recovery is initiated (i.e. the corner of the transition ramp) occurs further downstream with increasing mesh refinements which shows a delay in the transition of the separated BL. This is due to an alteration of the K-H roll simulation in the LSB and is the desired improvement from the mesh refinement, however the transition still occurs at an earlier x/c location when compared with the experimental data. The Mesh 2

and Mesh 3 simulations also resulted in a delay in reattachment of $0.06c$ in comparison with the Mesh 1 prediction. Though the C_p agreement from any of the tested mesh versions could be considered sufficient for validation of the time-averaged parameters, the BL frequency analysis in a later section will show that the 5° AOA case requires further mesh refinements and is still sensitive to changes in the BL mesh.

B. Flow Structure Visualization

The instantaneous BL behaviour at the TE of the airfoil is visualized in Fig. 6 which shows the Q-criterion isosurface at a value of $5 \times 10^7\ s^{-2}$ for the final time step of the Mesh 2 simulation for each AOA. The flow direction is from lower left to upper right and the surface is coloured with the non-dimensional velocity magnitude $|V|/U_\infty$ to highlight the height and shape of the structures and labels S and R are included to correspond to the locations of separation and reattachment in Fig. 5. The spanwise structures visualized in the regions of BL separation are the K-H rolls, which form due to the K-H instability in the separated BL. In a fully-formed LSB, such as the 5° AOA simulation, the K-H rolls breakdown into smaller 3D structures to complete the BL transition to turbulence and cause the BL to reattach to the airfoil surface. After breakdown and BL reattachment, the high spanwise coherence of the K-H rolls disappears resulting in a turbulent BL at the airfoil TE. For the 1° and 3° AOA simulations, the BL does not fully reattach before the TE and no significant K-H roll breakdown occurs. This high spanwise coherence can be seen in the structures visualized in the near wake of the airfoil, particularly for 1° AOA. This has implications for the tonal noise generation by the airfoil TE, where the cases with limited K-H roll breakdown and therefore high spanwise coherence will have TE pressure fluctuations occurring at the frequency with which the K-H rolls pass the TE.

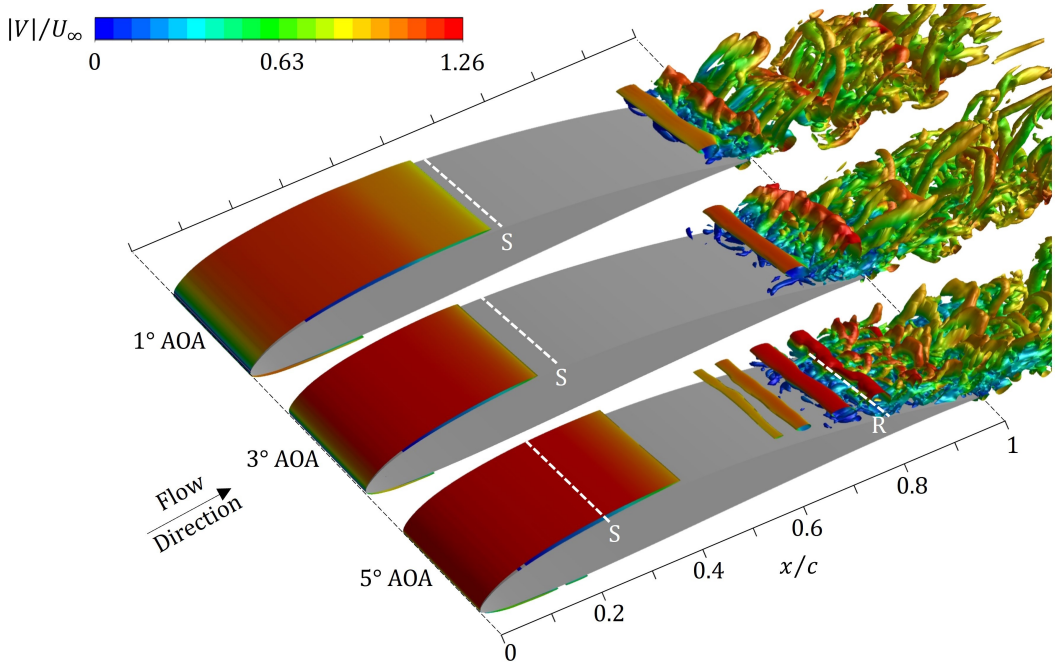

Fig. 6 Q-Criterion iso-surface of $5 \times 10^7\ s^{-2}$ for 1°, 3° and 5° AOAs using Mesh 2, coloured by non-dimensional velocity magnitude. White dashed lines indicate location of BL separation (S) and reattachment (R), where applicable

C. Boundary Layer Spectra

The simulation of the transient BL behaviour is assessed using the spectra of the wall-normal velocity, n-velocity, to isolate the frequencies of the instabilities present in the transitioning BL. The velocity was measured for 1×10^4 time steps at a wall-normal distance of $4 \times 10^{-3}c$ in the attached BL and a wall-normal distance of $3 \times 10^{-2}c$ in the LSB. The attached BL spectra for each case was collected at the location of laminar separation, rounded to the nearest $0.05c$, labelled S in Fig. 5. The spectra in the separated BL was collected $0.1c$ upstream of location of BL transition where the transition location was determined using maximum shape factor, H, and aligns with the location where C_p recovery is

initiated. For the 1° AOA simulations, transition did not occur before reaching the airfoil TE and instead a location $0.15c$ upstream of the TE was used for the spectral analysis.

1. 1° AOA

The 1° AOA n-velocity spectra are presented in Fig. 7 with the spectra in the attached BL measured at $x/c = 0.55$ and in the separated BL at $x/c = 0.85$. The transitional BL spectra in Fig. 7a has an elevated amplitude of n-velocity fluctuations centered around a frequency of $f = 3.5$ kHz for both Mesh 1 and 2, and the Mesh 1 spectra has some elevated amplitudes in the range of 4.2 to 8.5 kHz. At the location of BL separation, there are no identifiable flow structures present in the BL and the velocity fluctuations are at a very low amplitude of $n' = 0.2$ mm/s (0.3% of the local $\bar{n}$) and has corresponding s-velocity fluctuations at $s' = 15$ mm/s or 0.7% of the local $\bar{s}$. The maximum s-velocity amplitude of T-S waves before breakdown has been measured at 0.3% to 1% of the free stream velocity [39] and the simulated s' value is 0.06% of U_∞, therefore the fluctuations are assumed to be a result of the early development of T-S waves in the attached BL. The frequency of these fluctuations is in excellent agreement with the experimentally measured tonal noise for the airfoil, which is at $f = 3.4$ kHz [28], and are therefore determined to be physical phenomena of the transitioning BL rather than numerical error. It is also important to re-emphasize that the LES simulations are completed in the incompressible form, and therefore there can be no acoustic feedback triggering this instability, as the simulation does not resolve the propagation of acoustic waves in a direct manner.

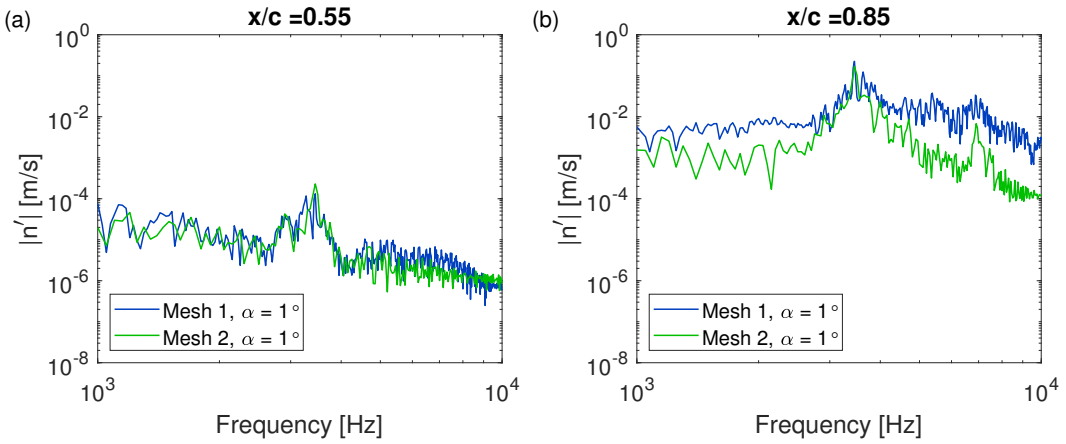

Fig. 7 Suction side of n-velocity spectra for 1° AOA for Mesh 1 and 2 at (a) $x/c = 0.55$ and a wall-normal distance of $4 \times 10^{-3}c$ and (b) $x/c = 0.85$ and a wall-normal distance of $3 \times 10^{-2}c$

The impact of the mesh refinement becomes apparent when comparing the frequencies present in the K-H rolls upstream of the TE in Fig. 7b, where the Mesh 2 refinements to the region of K-H roll development has changed the amplitudes of velocity fluctuation. In both Mesh 1 and 2, there is a dominant frequency at 3.5 kHz, which is due to the regular spacing of the K-H rolls in the separated BL, as well as the harmonic of this frequency at 6.9 kHz. The Strouhal number, $St_{\theta s}$, for the K-H roll frequency in the LSB is 0.010 for Mesh 1 and 0.009 for Mesh 2, which is in agrement with the range of 0.005 to 0.016 observed in other works [9]. However, the Mesh 1 spectra has a higher amplitude of velocity fluctuations for the entire frequency range which indicates that the K-H roll breakdown is beginning and the broadband fluctuations associated with a turbulent BL are occurring. There is also an additional frequency at 5.4 kHz in Mesh 1 that is not present in the Mesh 2 simulation. The changes to the development of the K-H rolls in the separated BL due to the mesh refinements has altered the frequency content of the BL as it approaches the TE. The impact on the tonal noise prediction from this change will be discussed in the next section.

The dominant frequency of the K-H rolls in the separated BL is identical to the T-S frequency measured in the attached BL which points to a strong relationship between the two behaviours. Previous researchers have also found a similarity between the T-S and K-H frequencies, and hypothesized of the interaction between the behaviours [8, 9]. Brinkerhoff and Yaras [9] applied DNS to a LSB on a flat plate and performed a test case with and without the LSB to determine that the T-S frequency in the attached BL developed at the given frequency independently of the K-H instability in the LSB. Therefore the K-H instability can be said to amplify any existing T-S frequency that is present in the BL at the point of laminar separation. In the 1° AOA simulations, the T-S frequency is present at very low amplitudes

from the airfoil LE and grows to the amplitude seen in Fig. 7a at laminar separation. This highlights the importance of the mesh resolution near the wall at the airfoil LE, where the BL thickness is low and the velocity gradients are high. If the incorrect T-S frequency develops in the attached BL, then the amplification of that frequency through the K-H instability will lead to incorrect frequency behaviour at the airfoil TE and therefore an incorrect tonal noise prediction.

2. 3° AOA

The behaviour present in the 3° AOA n-velocity spectra in Fig. 8 follows a similar pattern to the results for 1° AOA. In the spectra measured at the location of laminar separation, $x/c = 0.45$, there is a dominant tone present at a frequency of 3.0 kHz which is again assumed to be the T-S wave frequency. The same dominant frequency is present in the measurements in the separated BL at $x/c = 0.75$, which is $0.1c$ upstream of the transition location of the separated BL. Therefore the frequency of the K-H rolls is also 3.0 kHz, and corresponds to a Strouhal number of $St_{\theta s} = 0.006$ for Mesh 2 and $St_{\theta s} = 0.007$ for Mesh 3, which are both within the reported range [9]. When comparing the spectra in the separated BL, the additional refinements in the region of K-H roll development in Mesh 3 has resulted in a lower amplitude of velocity fluctuations, again indicating less K-H roll breakdown occurring in the Mesh 3 simulation. This minimal level of change in the n-velocity spectra in the K-H rolls is expected since the Mesh 2 filter length in the K-H roll region of the mesh is close to meeting the 3° AOA l_{EI} criterion (Fig. 4b), and Mesh 3 exceeds the criterion by a similar amount.

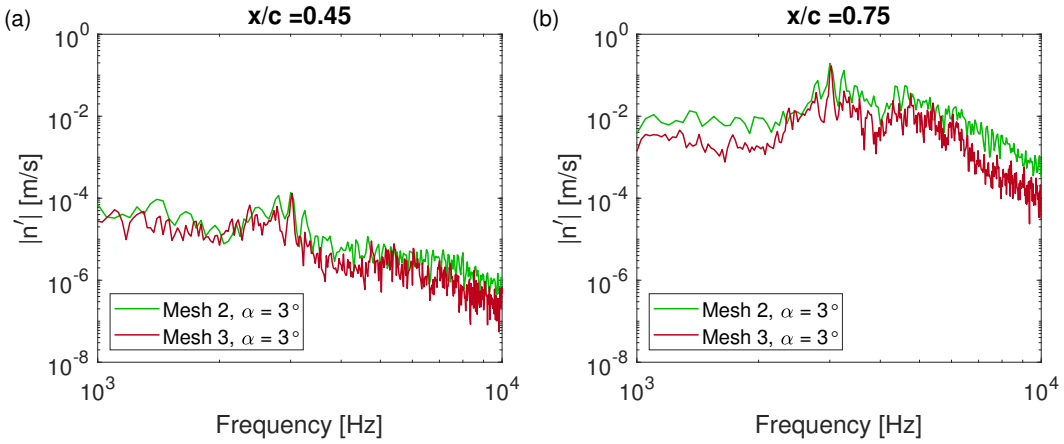

Fig. 8 Suction side of n-velocity spectra for 3° AOA for Mesh 2 and 3 at (a) $x/c = 0.45$ and a wall-normal distance of $4 \times 10^{-3}c$ and (b) $x/c = 0.75$ and a wall-normal distance of $3 \times 10^{-2}c$

3. 5° AOA

In contrast to the previous AOAs, the 5° AOA n-velocity spectra in Fig. 9 shows significant variation with each of the mesh versions. The spectra at the separation location of $x/c = 0.3$ does not show a dominant tone associated with the T-S wave formation, and rather has a series of broadband humps centered around frequencies ranging from 2.9 kHz in Mesh 1 to 7.9 kHz in Mesh 3. The amplitude of the velocity fluctuations at those frequencies are amplified in the separated BL at a location of $x/c = 0.55$, which occurs in the same manner as the T-S frequency amplification in the 1° and 3° AOA simulations. The resulting Strouhal numbers for the K-H roll frequencies are $St_{\theta s} = 0.008$ for Mesh 1, $St_{\theta s} = 0.010$ for Mesh 2 and $St_{\theta s} = 0.011$ for Mesh 3, which are still within the reported range [9]. The broadband nature of the frequencies present in the K-H rolls for the different mesh versions can be visualized in the Q-criterion of Fig. 6 for Mesh 2 at 5° AOA. The visualized K-H rolls appear at inconsistent chordwise spacing, which would result in a wider range of frequencies in the n-velocity spectra in comparison to the dominant frequencies seen for 1° and 3° AOA.

Additionally, the experimental acoustic measurements [28] at 5° AOA identifies a similar dominant tone of 3.3 kHz to the 3.4 kHz tone measured for 1° AOA . For this reason, it would be expected that a similar T-S wave frequency and K-H amplification of the frequency should occur in the 5° AOA case. It is known from the filter length comparison in Fig. 4a that the filter length for the K-H roll region of the mesh is likely insufficient, but the inaccuracy in the T-S wave frequency implies that the near-wall mesh in the laminar BL requires further refinement as well.

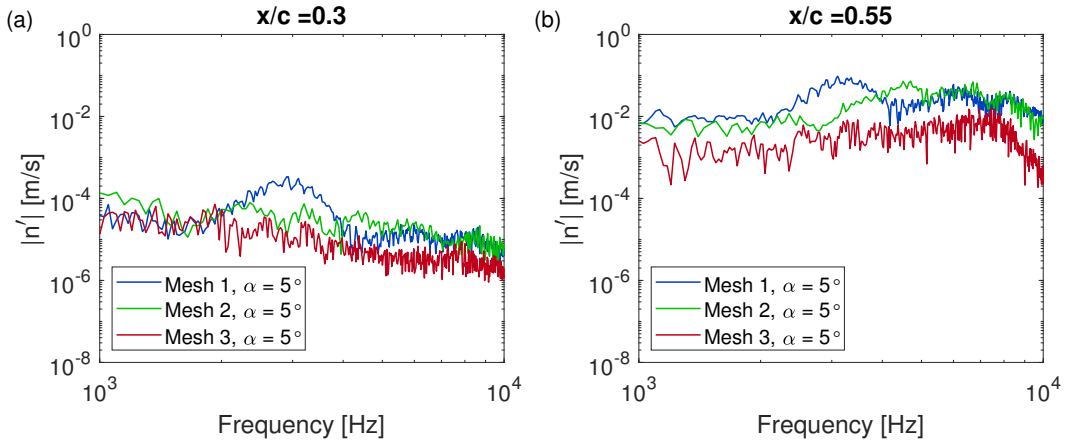

Fig. 9 Suction side of n-velocity spectra for 5° **AOA for Mesh 1, 2 and 3 at (a)** $x/c = 0.3$ **and a wall-normal distance of** $4 \times 10^{-3}c$ **and (b)** $x/c = 0.55$ **and a wall-normal distance of** $3 \times 10^{-2}c$

D. Aeroacoustic Spectra

The narrowband sound pressure level (SPL) spectra predicted by the FW-H model for each simulation are shown in Fig. 10 and are compared with the measured experimental spectra [28]. The SPL spectra was generated through an ensemble average of the FFTs of each acoustic pressure signal divided into two equal segments. Since the simulated span is 3.4% of the experimental span, the predicted acoustic pressure amplitudes were multiplied by 29.5 before conversion to SPL to be representative of the noise produced by the entire experimental span.

The dominant tone at 1° AOA, shown in Figure 10a, is accurately predicted at a frequency of 3.5 kHz with a SPL of 84 dB for Mesh 1 and 87 dB for Mesh 2, in comparison to the experimental tone at a frequency of 3.4 kHz and a SPL of 122 dB. It should be noted that the acoustic experiments were completed in a closed loop wind tunnel with acoustic treatments [28], rather than an anechoic tunnel, which could have resulted in an artificial increase in the experimental tone SPL due to reflection within the wind tunnel test section.

When comparing the dominant tone frequency from Mesh 1 and 2 to the dominant frequency of 3.5 kHz from the n-velocity spectra in the airfoil BL, the source of the tonal noise can be definitively connected to the K-H rolls formed in the separated BL on the suction side of the airfoil. The rotation of the K-H rolls, which are visualized in Fig. 6, results in low pressure at the centre of each roll and high pressure between each successive roll. Since the K-H rolls have a high spanwise coherence, the entire span of the airfoil TE alternates between low and high pressure as the K-H rolls are shed and therefore there is a consistent pressure fluctuation scattered to the farfield receiver location. The n-velocity spectra also showed that the K-H rolls develop at the same frequency as the T-S waves in the attached laminar BL, and it is the amplification of the T-S wave amplitude through the K-H instability that results in the loud tonal noise at the TE. This amplification of the T-S wave amplitude occurs in the simulations without the presence of acoustic feedback since the incompressible LES method is unable to directly predict the propagation of acoustic waves or their interference with the development of the transitional BL.

The improvements in the acoustic prediction from the mesh refinements in the K-H roll region of Mesh 2 can be seen when examining the SPL of the secondary tone of 4.1 kHz [28], where Mesh 1 has an over-prediction of the tone with a SPL of 73 dB at 4.0 kHz and Mesh 2 predicts a quieter tone of 65 dB at 4.1 kHz. Prior examination of the Mesh 2 results [40] has shown an intermittency of the 4.1 kHz tone related to the presence of a spanwise instability in the K-H rolls as they pass the airfoil TE. The primary 3.4 kHz tone occurs when the K-H rolls maintain high spanwise coherence and the secondary tone occurs during the intermittent initiation of spanwise breakdown in the K-H rolls near the TE. Therefore the elevated SPL of the 4.0 kHz tone predicted by Mesh 1 is related to a more frequent occurrence of spanwise breakdown of the K-H rolls. The examination of the n-velocity spectra in the separated BL in Fig. 7 showed that the Mesh 1 K-H rolls begin the breakdown earlier in the LSB than the Mesh 2 K-H rolls, further validating the K-H roll breakdown as the source of the higher SPL of the 4.1 kHz tone. The mesh refinements in the K-H roll region to meet the filter length criterion of l_{EI} are therefore necessary to generate a correct aeroacoustic prediction of the tonal noise, since variations in the prediction of the location and intermittency of K-H roll breakdown will alter the tonal frequencies present at the airfoil TE.

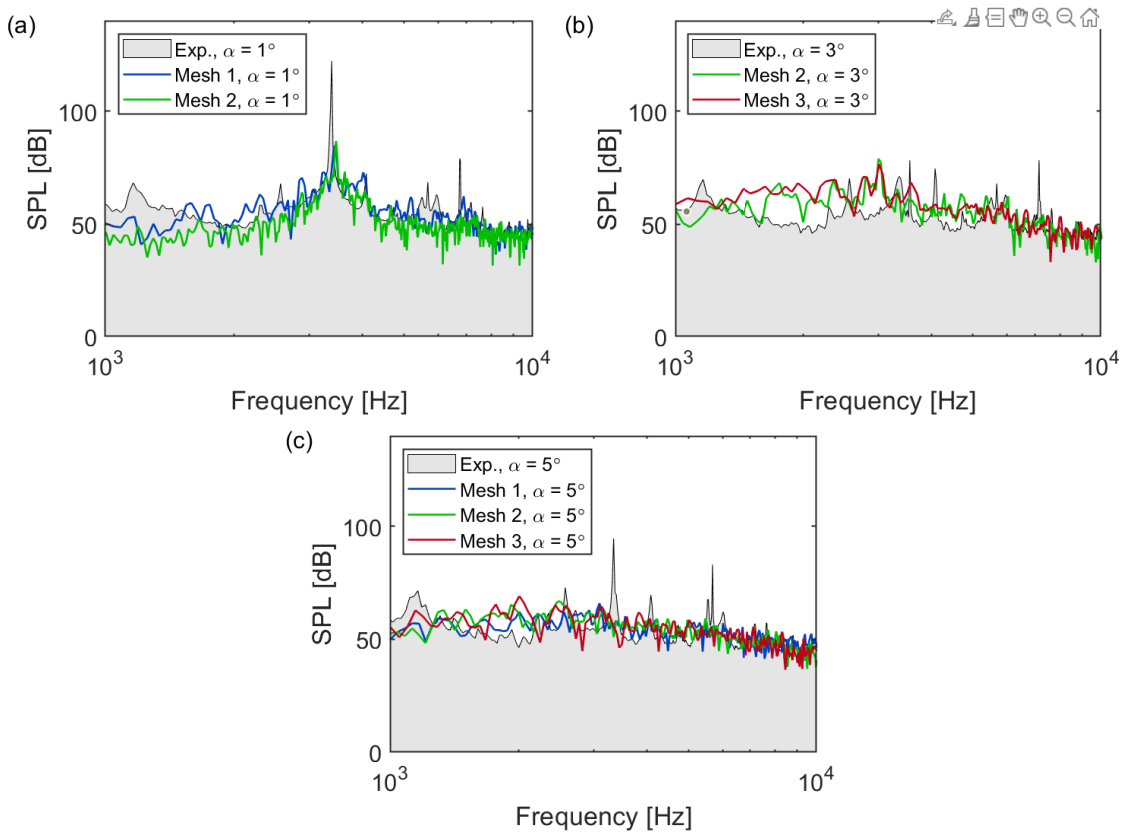

Fig. 10 Acoustic SPL spectra for (a) 1° AOA, (b) 3° AOA and (c) 5° AOA compared with experimental measurements [28] for Mesh 1 to 3

The 3° AOA acoustic spectra in Fig. 10b predict a dominant tone at 3.0 kHz and a SPL of 79 dB for Mesh 2 and 77 dB for Mesh 3. This tone frequency is in agreement with the K-H and T-S frequency detected in the suction side BL in Fig. 8, and therefore the same mechanism generates the tonal TE noise for 1° and 3° AOAs. However, the dominant tonal frequency predicted by the 3° AOA simulations is 0.4 kHz lower than the tone frequency found experimentally [28] and in the 1° AOA simulation, which requires further investigation and may indicate that additional mesh refinements are necessary to develop the appropriate T-S frequency in the attached laminar BL. The K-H roll visualization in Fig. 6 for the 3° AOA Mesh 2 simulation shows the initiation of the breakdown of K-H rolls although the structures maintain a high spanwise coherence at the TE of the airfoil. This increased breakdown in comparison with the 1° AOA simulation results in a lower tonal noise SPL and an increased SPL of the broadband spectra, which is associated with the random fluctuations of the increased turbulence in the 3° AOA BL.

The acoustic spectra prediction in Fig. 10c for all three mesh versions at 5° AOA is unable to detect any tonal noise in comparison with the experimental tone measurement of 95 dB at a frequency of 3.3 kHz [28]. The n-velocity spectra in Fig. 9b contained several broadband humps associated with the variation in the shedding frequency of the K-H rolls, however that spectra is measured at $x/c = 0.55$ and significant breakdown of the K-H rolls occurs after that location. This is visualized in Fig. 6 for Mesh 2, where there is no spanwise coherence of the BL structures after the location of BL reattachment. The tonal noise expected from this AOA based on the experimental acoustic spectra would require spanwise coherence of the structures in the reattached BL to generate the correct level of acoustic scattering at the TE. The absence of a dominant T-S frequency and K-H frequency in the n-velocity spectra already indicated the need for further mesh refinements, and the need for these refinements is further indicated by the absence of tonal noise in the predicted acoustic spectra.

IV. Conclusion

The prediction of tonal aeroacoustic noise generated by the TE of the SD 7037 airfoil at a modest Re of 4.1×10^4 was successfully completed using incompressible wall-resolved LES and the FW-H acoustic analogy. A series of three mesh versions were used to refine the mesh resolution and associated LES filter length in the attached laminar BL and in the regions of K-H roll development in the LSB. These refinements were found to improve the accuracy of the tonal noise prediction at 1° AOA, where the refined mesh in the region of K-H roll development reduced the intermittency of the K-H roll breakdown in the LSB to better predict the tonal noise at the airfoil TE. These improvements to the transient behaviour of the BL transition structures occurred without alteration of the time-averaged BL properties, such as C_p, highlighting the challenge of accurately validating the LES simulation when the results are to be used for aeroacoustic noise predictions.

The analysis of the spectral content of the n-velocity in the BL at the location of laminar separation and in the separated BL showed that the tonal noise frequency originates from the T-S wave frequency in the attached BL and is amplified through the K-H instability in the separated BL. This process occurred in the absence of acoustic feedback due to the incompressible form of the simulations, which do not capture the upstream propagation of acoustic waves. In the case of the 3° and 5° AOA simulations, the frequencies in the attached BL amplified by the K-H instability was not in agreement with the experimental tonal noise frequencies and therefore resulted in an incorrect tonal noise prediction. Further tightening of the mesh criteria in the laminar BL and in the region of K-H roll development are required to improve the tonal noise prediction at higher AOAs where the LSB is located upstream of the TE. For the 1° AOA simulation, the current mesh criteria were sufficient to resolve the transient behaviour of a low Re airfoil with a LSB located at the TE and resulted in the correct prediction of the tonal noise generated by the K-H rolls in the separated BL.

Acknowledgments

Funding for this research is provided in part by the Natural Sciences and Engineering Research Council of Canada (NSERC) through Discovery Grant No. RGPIN-2023-04136. The NSERC Alexander Graham Bell Canada Graduate Scholarship-Doctoral (CGS-D) was also awarded to Alison Zilstra as a doctoral scholarship. The authors would like to acknowledge the dedicated effort of Faegheh Ghorbanishohrat and Nicholas Tam to produce the high quality experimental data used to validate these results.

References

[1] Brooks, T. F., Pope, D. S., and Marcolini, M. A., "Airfoil self-noise and prediction," Tech. Rep. NASA-RP-1218, NASA Reference Publication, 1989. URL http://ntrs.nasa.gov/archive/nasa/casi.ntrs.nasa.gov/19890016302.pdf.

[2] Wagner, S., Bareiss, R., and Guidata, G., *Wind Turbine Noise*, Springer-Verlag Berlin Heidelberg, Berlin, 1996.

[3] Winkler, J., Wu, H., Moreau, S., Carolus, T., and Sandberg, R. D., "Trailing-edge broadband noise prediction of an airfoil with boundary-layer tripping," *Journal of Sound and Vibration*, Vol. 482, 2020, pp. 1–25. https://doi.org/10.1016/j.jsv.2020.115450.

[4] Tani, I., "Low-speed flows involving bubble separations," *Progress in Aerospace Sciences*, Vol. 5, No. C, 1964, pp. 70–103. https://doi.org/10.1016/0376-0421(64)90004-1.

[5] Schlichting, H., and Gersten, K., *Boundary-Layer Theory*, 9th ed., Springer-Verlag Berlin Heidelberg, 2017.

[6] Yuan, W., Khalid, M., Windte, J., Scholz, U., and Radespiel, R., "An investigation of Low-Reynolds-number flows past airfoils," *Collection of Technical Papers - AIAA Applied Aerodynamics Conference*, Vol. 1, No. April 2015, 2005, pp. 102–120. https://doi.org/10.2514/6.2005-4607.

[7] Zilstra, A., and Johnson, D. A., "Large Eddy Simulation of Transitional Separated Flow Over a Low Reynolds Number Cambered Airfoil," *Journal of Fluids Engineering*, Vol. 145, No. 3, 2023. https://doi.org/10.1115/1.4056280.

[8] Hain, R., Kahler, C. J., and Radespiel, R., "Dynamics of laminar separation bubbles at low-Reynolds-number aerofoils," *Journal of Fluid Mechanics*, Vol. 630, 2009, p. 129–153. https://doi.org/10.1017/S0022112009006661.

[9] Brinkerhoff, J. R., and Yaras, M. I., "Interaction of viscous and inviscid instability modes in separation-bubble transition," *Physics of Fluids*, Vol. 23, No. 12, 2011. https://doi.org/10.1063/1.3666844.

[10] Walker, G. J., "Transitional flow on axial turbomachine blading," *AIAA Journal*, Vol. 27, No. 5, 1989, pp. 595–602. https://doi.org/10.2514/3.10150.

[11] Wissink, J. G., and Rodi, W., "Direct Numerical Simulations of Transitional Flow in Turbomachinery," *Journal of Turbomachinery*, Vol. 128, No. 4, 2006, pp. 668–678. https://doi.org/10.1115/1.2218517.

[12] Ghorbanishohrat, F., "Study of a low Re airfoil considering laminar separation bubbles in static and pitching motion," Ph.D. thesis, University of Waterloo, 2019. URL http://hdl.handle.net/10012/14428.

[13] Zilstra, A., and Johnson, D. A., *25th AIAA/CEAS Aeroacoustics Conference, 2019*, 2019, pp. 1–13. https://doi.org/10.2514/6.2019-2537.

[14] Deuse, M., and Sandberg, R. D., "Different noise generation mechanisms of a controlled diffusion aerofoil and their dependence on Mach number," *Journal of Sound and Vibration*, Vol. 476, 2020. https://doi.org/10.1016/j.jsv.2020.115317.

[15] Lighthill, M., "On sound generated aerodynamically I. General theory," *Proceedings of the Royal Society of London. Series A. Mathematical and Physical Sciences*, Vol. 211, No. 1107, 1952, pp. 564–587. https://doi.org/10.1098/rspa.1952.0060.

[16] Crighton, D. G., "Computational Aeroacoustics for Low Mach Number Flows," *Computational Aeroacoustics*, Springer-Verlag New York, New York, 1993, Chap. Classical, pp. 50–68. https://doi.org/10.1007/978-1-4613-8342-0_3.

[17] Farassat, F., "The Acoustic Analogy as a Tool of Computational Aeroacoustics," *Computational Aeroacoustics*, Springer-Verlag New York, 1993, Chap. Mathematical Aspects of Acoustics, pp. 133–155. https://doi.org/10.1007/978-1-4613-8342-0_7.

[18] Ffowcs Williams, J., and Hawkings, D., "Sound Generation by Turbulence and Surfaces in Arbitrary Motion," *Philisophical Transactions of the Royal Society of London. Series A, Mathematical and Physical Sciences*, Vol. 264, No. 1151, 1969, pp. 321–342.

[19] Brentner, K. S., and Farassat, F., "Analytical Comparison of the Acoustic Analogy and Kirchhoff Formulation for Moving Surfaces," *AIAA Journal*, Vol. 36, No. 8, 1998, pp. 1379–1386. https://doi.org/10.2514/2.558.

[20] Smith, T. A., and Ventikos, Y., "Boundary layer transition over a foil using direct numerical simulation and large eddy simulation," *Physics of Fluids*, Vol. 31, No. 12, 2019. https://doi.org/10.1063/1.5126663.

[21] Thomareis, N., and Papadakis, G., "Effect of trailing edge shape on the separated flow characteristics around an airfoil at low Reynolds number A numerical study," *Physics of Fluids*, Vol. 29, No. 1, 2017. https://doi.org/10.1063/1.4973811.

[22] Jones, L. E., Sandberg, R. D., and Sandham, N. D., "Direct numerical simulations of forced and unforced separation bubbles on an airfoil at incidence," *Journal of Fluid Mechanics*, Vol. 602, 2008, pp. 175–207. https://doi.org/10.1017/S0022112008000864.

[23] Ziadé, P., Feero, M. A., Lavoie, P., and Sullivan, P. E., "Shear Layer Development, Separation, and Stability Over a Low-Reynolds Number Airfoil," *Journal of Fluids Engineering*, Vol. 140, No. 7, 2018, pp. 1–12. https://doi.org/10.1115/1.4039233.

[24] Lardeau, S., Leschziner, M., and Zaki, T., "Large Eddy Simulation of Transitional Separated Flow over a Flat Plate and a Compressor Blade," *Flow, Turbulence and Combustion*, Vol. 88, No. 1-2, 2012, pp. 19–44. https://doi.org/10.1007/s10494-011-9353-0.

[25] Galbraith, M. C., and Visbal, M. R., "Implicit large eddy simulation of low-Reynolds-number transitional flow past the SD7003 airfoil," *46th AIAA Aerospace Sciences Meeting and Exhibit*, 2008. https://doi.org/10.2514/6.2010-4737.

[26] Breuer, M., "Effect of Inflow Turbulence on an Airfoil Flow with Laminar Separation Bubble: An LES Study," *Flow, Turbulence and Combustion*, Vol. 101, No. 2, 2018, pp. 433–456. https://doi.org/10.1007/s10494-017-9890-2.

[27] Zilstra, A., and Johnson, D. A., "Computational aeroacoustic prediction of trailing edge noise for small wind turbines," *Journal of Physics: Conference Series*, Vol. 1618, No. 4, 2020, p. 042010. https://doi.org/10.1088/1742-6596/1618/4/042010.

[28] Tam, N., "An Aeroacoustic Study of Airfoil Self-Noise for Wind Turbine Applications," Master's thesis, University of Waterloo, 2017. URL http://hdl.handle.net/10012/11736.

[29] SHARCNET, "Digital Research Alliance of Canada," , 2024. URL https://alliancecan.ca/en.

[30] Selig, M. S., Lyon, C. A., Giguere, P., Ninham, C. P., and Guglielmo, J., *Summary of low-speed airfoil data, Vol. 2*, SoarTech Publications, VA, 1996.

[31] Lobo, B. A., Schaffarczyk, A. P., and Breuer, M., "Investigation into boundary layer transition using wall-resolved large-eddy simulations and modeled inflow turbulence," *Wind Energy Science*, Vol. 7, No. 3, 2022, pp. 967–990. https://doi.org/10.5194/wes-7-967-2022.

[32] Versteeg, H., Malalasekera, W., Orsi, G., Ferziger, J. H., Date, A. W., and Anderson, J. D., *An Introduction to Computational Fluid Dynamics - The Finite Volume Method*, 2nd ed., Pearson Education Limited, Harlow, 1995. https://doi.org/10.2514/1.22547.

[33] Dhamankar, N. S., Blaisdell, G. A., and Lyrintzis, A. S., "Overview of turbulent inflow boundary conditions for large-eddy simulations," *AIAA Journal*, Vol. 56, No. 4, 2018, pp. 1317–1334. https://doi.org/10.2514/1.J055528.

[34] Roberts, S. K., and Yaras, M. I., "Large-Eddy Simulation of Transition in a Separation Bubble," *Journal of Fluids Engineering*, Vol. 128, No. 2, 2006, pp. 232–238. https://doi.org/10.1115/1.2170123.

[35] Orlando, S. M., "Laser Doppler Anemometry and Acoustic Measurements of an S822 Airfoil at Low Reynolds Numbers," Master's thesis, University of Waterloo, 2011. URL http://hdl.handle.net/10012/5864.

[36] ANSYS Academic Research, Release 20.2, "ANSYS Fluent Theory Guide," *ANSYS Help System*, ANSYS Inc., Release 20.2, 20th ed.

[37] Pope, S. B., *Turbulent Flows*, Cambridge University Press, 2000.

[38] Russell, J. M., *Length and Bursting of Separation Bubbles: A Physical Interpretation*, NASA. Langley Res. Center The Sci. and Technol. of Low Speed and Motorless Flight, Pt. 1, 1979. URL https://ntrs.nasa.gov/archive/nasa/casi.ntrs.nasa.gov/19790015727.pdf.

[39] White, F. M., *Viscous Fluid Flow*, 2nd ed., McGraw Hill, New York, 1991.

[40] Zilstra, A., and Johnson, D. A., "Numerical Prediction of Tonal Aeroacoustic Noise Produced by Small Wind Turbines," *Journal of Physics: Conference Series*, 2024.